(Received 13 January 2025, Accepted 20 February 2025, Scheduled 4 March 2025)

A Miniaturized Circularly Polarized Microstrip Antenna Utilizing Meandering Technique and Minkowski-Sierpinski Fractal Structure

Lin Wang[1,2], Liang Zhang[2,1,*], Lixia Yang[1], Xinyan Wang[1,2], Xialin Sheng[1,2], Quan Jin[1,2], and Po Tian[1,2]

[1] *School of Electronic and Information Engineering, Anhui University, Hefei 230601, China*
[2] *Anhui Province Key Laboratory of Simulation Calculation and Design for Electronic Information System Hefei Normal University, Hefei 230601, China*

ABSTRACT: In this paper, we present a miniaturized design of a microstrip antenna achieved through the combination of Minkowski-Sierpinski (M-S) fractal structure and meandering technique, enabling the antenna to be integrated into smaller systems. The antenna achieves right-hand circular polarization (RHCP) through chamfering on a square patch. Further miniaturization is accomplished by loading four symmetrically opposed L-shaped slots along with the M-S fractal structure. Specifically, the Minkowski structure undergoes a single iteration, while the Sierpinski fractal is iterated twice on the once-iterated Minkowski fractal to optimize performance. The antenna is manufactured on a textile substrate TLX-8 with dimensions of 50 mm × 50 mm × 0.762 mm, representing a 54.3% reduction in size compared to traditional designs. Moreover, the substrate exhibits robust mechanical properties. Experimental results demonstrate that the antenna achieves excellent radiation characteristics within a bandwidth of 1.563 to 1.581 GHz and an axial ratio bandwidth of 1.569 to 1.578 GHz. These performance metrics meet the requirements for modern Global Positioning System (GPS) antenna applications, highlighting the design's suitability for advanced integration in contemporary electronic systems.

1. INTRODUCTION

As antenna technologies advance and system integration levels escalate, the market demand for miniaturized antennas is increasingly prominent. Consequently, the exploration of antenna miniaturization techniques has become a focal point in both academic research and industrial development [1, 2]. The primary objective is to reduce the physical dimensions of antennas while preserving their performance, thereby meeting the stringent requirements of progressively compact device designs.

In the realm of antenna miniaturization research, prevalent strategies include the utilization of high-dielectric-constant substrates, meandering technique, fractal geometries, and the application of metamaterials. Specifically, Ref. [3] illustrates the successful reduction of a GPS antenna to dimensions of 50 mm × 37 mm × 5.8 mm by employing a dielectric substrate with a relative permittivity of 6.5. Additionally, Ref. [4] describes an innovative parasitic metamaterial structure that was loaded in the near-field region of the antenna, effectively reducing the antenna size by 52.94%. Although these methods demonstrate significant efficacy in reducing antenna dimensions, they also result in substantial increases in design costs, complexity, and difficulty. In practical implementations, these technologies may face challenges related to cost-effectiveness and manufacturability.

Meandering technique in antenna design involves etching various geometric shapes onto a single layer or patch, with the fundamental principle of miniaturizing the antenna by elongating the surface current path. In [5], a novel asymmetric-circularly slotted microstrip patch antenna is proposed. By embedding asymmetric-circular slots along the diagonal of a square microstrip patch and introducing four symmetrically placed slits at the patch edges, the antenna achieves circular polarization and miniaturization. In contrast, the design in [6] employs a different strategy by embedding asymmetric square ring slots along the diagonal of a square patch, resulting in a miniaturized circular polarization (CP) antenna with dimensions of 60 mm × 60 mm × 5 mm operating at 1575 MHz. Both designs demonstrate significant size reduction while maintaining antenna performance through structural optimization. Ref. [7] introduces a CP antenna incorporating F-shaped slots and defected ground structures (DGSs), achieving both miniaturization and enhanced axial ratio (AR) bandwidth. Both [8] and [9] propose innovative slotted microstrip antenna designs to achieve miniaturized CP. Specifically, Ref. [8] introduces an antenna with dimensions of 36 mm × 36 mm × 1.524 mm by embedding asymmetric triangular slots at the four corners of a square patch. This design leverages the asymmetry to optimize the radiation performance while significantly reducing the antenna size. In contrast, Ref. [9] employs symmetric triangular and square slots, combined with corner truncation techniques,

* Corresponding author: Liang Zhang (liangzh@hfnu.edu.cn).

to achieve miniaturization and CP in an antenna of the same dimensions.

Fractal structures have garnered significant interest among antenna researchers due to their self-similarity and space-filling properties [10, 11]. Mandelbrot [12] was the first to introduce the concept of fractal geometry. Subsequently, various fractal antenna designs have been proposed in the literature, including Minkowski fractal, Sierpinski fractal, and Koch curve geometry [13–15]. As research has progressed, numerous combinations of fractal structures have emerged. For instance, Ref. [16] presents a novel hybrid fractal antenna combining Koch and Minkowski geometries (K-M fractal), achieving a 20% reduction in antenna size. However, this design suffers from excessive iteration steps, resulting in increased design complexity and computational demands that limit its practical applications. Furthermore, Ref. [17] describes an M-S fractal antenna array that uses a Wilkinson power divider for equal power distribution, thus constructing the feed network. Although this design offers excellent radiation characteristics and is widely used in wireless local area network (WLAN) applications, it also exhibits drawbacks such as complex design procedures and relatively large physical dimensions.

To address the above problems, this study introduces an antenna design that combines meandering techniques with fractal geometries. The antenna utilizes four L-shaped slots symmetrically arranged in pairs at its center and employs a first-order Minkowski fractal alongside a second-order Sierpinski fractal in its design. A TLX-8 textile substrate with a dielectric constant of 2.55 is utilized, offering benefits such as a simple structure, low profile, and cost efficiency. The GPS, a key component of the Global Navigation Satellite System (GNSS), leverages satellite-based radio navigation technology extensively in military, civilian, and commercial applications. Given that GPS signals operate at a frequency of 1.57542 GHz within the L band, their relatively long wavelength requires larger physical antenna sizes in traditional designs [18]. Consequently, this research focuses the antenna design around the GPS operating frequency. Through both simulation and experimental validation, the antenna achieves dimensions of 50 mm × 50 mm × 0.762 mm, representing a 54.3% reduction compared to conventional sizes. It operates within a frequency range of 1.57 to 1.582 GHz and attains a maximum directional gain of 0.39 dBi. The strong agreement between simulation and measurement results demonstrates that the antenna meets the design requirements for contemporary GPS technologies.

2. ANTENNA DESIGN

2.1. Antenna Configuration

Figure 1 presents the planar structure of the antenna proposed in this study. The antenna is an improvement on a square patch that achieves CP through chamfering. Initially, four symmetric L-shaped slots of dimensions $l_x \times l_y$ are introduced at the center of the patch, leveraging the principles of meandering technology to achieve a low-frequency shift in the resonant frequency. Subsequently, a Minkowski fractal structure with a notch depth of L_m is loaded to further optimize the antenna's performance.

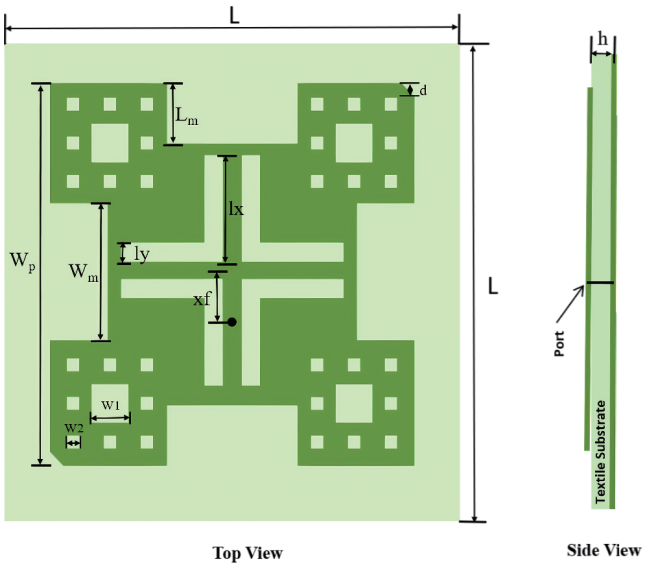

FIGURE 1. Geometry of the proposed antenna.

Finally, second-order Sierpinski fractal structures are loaded on the square sections at the four corners, with the first- and second-order opening dimensions being W_1 and W_2, respectively. The specific design process of the antenna patch is shown in Fig. 2. Additionally, the ground plane of the antenna is printed with a complete grounding plane to accommodate various metallic environments. The antenna is fabricated using a TLX-8 glass fiber substrate with dimensions of 50 mm × 50 mm × 0.762 mm, a relative permittivity of 2.55, and a loss tangent of 0.0017. This substrate not only exhibits excellent electrical properties but also possesses superior mechanical and thermal characteristics, making it suitable for a variety of complex operating environments. The specific parameters of the antenna are listed in Table 1.

TABLE 1. Geometrical parameters as well as values of antenna.

Antenna Dimensions	Value (Unit: mm)
L	50
W_p	40
h	0.762
xf	5.8
l_x	11.15
l_y	2
W_m	13.3
L_m	5.3
W_1	4.5
W_2	1.48
d	1.25

To more clearly illustrate the impact of each step in the antenna improvement process on performance trends, Fig. 3 presents the S-parameter plots for Ants. 1, 2, 3, and 4. Ant. 1 demonstrates good impedance matching at 2.3 GHz. The introduction of an L-shaped slot in Ant. 2 and the addition of a Minkowski fractal structure in Ant. 3 result in a significant shift

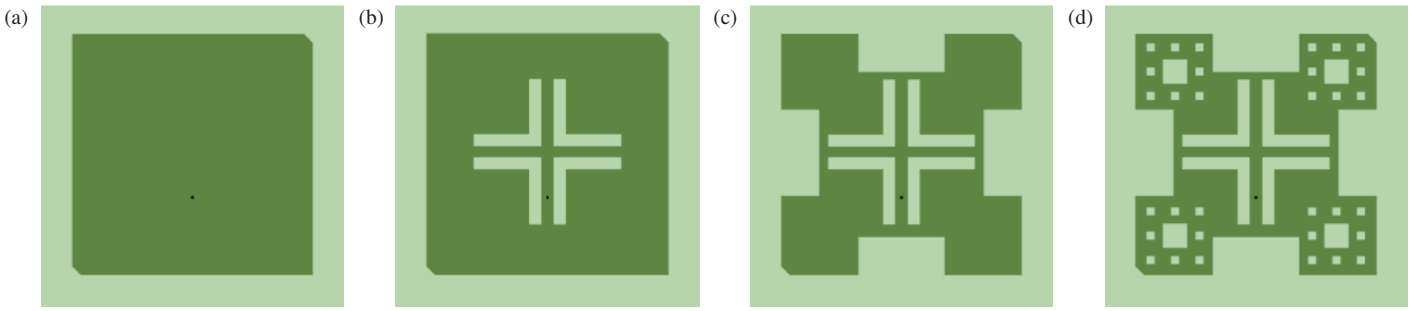

FIGURE 2. Design process of the proposed antenna. (a) Ant. 1. (b) Ant. 2. (c) Ant. 3. (d) Ant. 4.

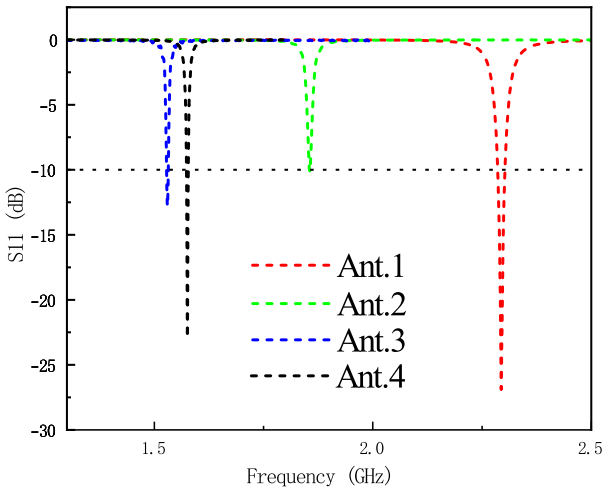

FIGURE 3. S_{11} of the proposed antenna for different structures.

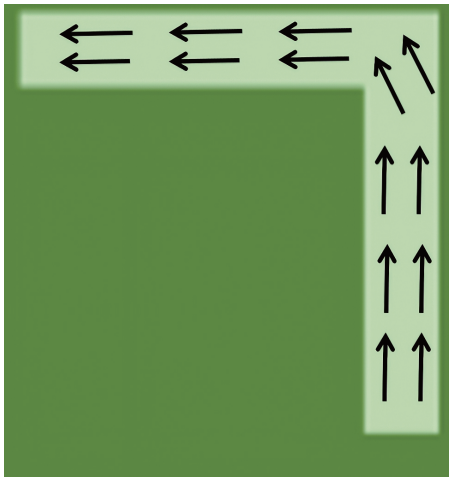

FIGURE 4. Schematic of meandering technique.

of the resonant frequency towards lower frequencies, achieving effective miniaturization. However, the impedance matching performance of both antennas deteriorates. Finally, Ant. 4, which incorporates a second-order Sierpinski fractal structure, shows improved impedance matching, achieving a center resonant frequency of 1.575 GHz.

2.2. Theoretical Analysis

Figure 4 depicts the pioneering application of the meandering technique to microstrip antennas, enabling a reduction in antenna dimensions through the optimization of the effective surface current path [19]. Additionally, the extension of the current path associated with the primary resonant mode leads to an elongation of the antenna's resonant wavelength, consequently reducing the resonant frequency of the patch. This method not only effectively diminishes the antenna's physical size but also refines its electrical properties by modulating the length of the current path, thereby enhancing its performance across a targeted frequency spectrum.

Fractal structures are typically generated through self-similar iterations of an initial unit according to a predetermined scaling factor. The initial unit determines the framework of the fractal pattern, while the iterative units define the internal structure of the fractal.

Figure 5 illustrates the iterative process of the Minkowski fractal structure. We employ a two-point method to generate this fractal loop [20]: initially, an initial unit and a generating unit are constructed. The initial unit represents the original structure, while the generating unit defines the transformation of the fractal. Two points are given in the complex plane with coordinates Z_0 and Z_1. The superscript "0" denotes the initial unit, and "1" indicates the generating unit; the subscript represents the order of the points.

The initial unit is defined as $Z_0 = Z_0^{(0)}$, $Z_1 = Z_1^{(0)}$; the generating unit is set as $Z_0^{(1)} = Z_0^{(0)}$, $Z_5^{(1)} = Z_0^{(0)}$, thereby:

$$\left|Z_1^{(1)} - Z_0^{(1)}\right| = \left|Z_3^{(1)} - Z_2^{(1)}\right| = \left|Z_5^{(1)} - Z_4^{(1)}\right| = \frac{1}{3}|Z_1^{(0)} - Z_0^{(0)}| \quad (1)$$

$$\left|Z_5^{(1)} - Z_1^{(1)}\right| = \left|Z_4^{(1)} - Z_3^{(1)}\right| = \left|Z_5^{(1)} - Z_4^{(1)}\right| = \frac{\alpha}{3}\left|Z_1^{(0)} - Z_0^{(0)}\right| \quad (2)$$

The generating unit segments are defined in relation to the initial unit, and the resulting values are expressed in terms of

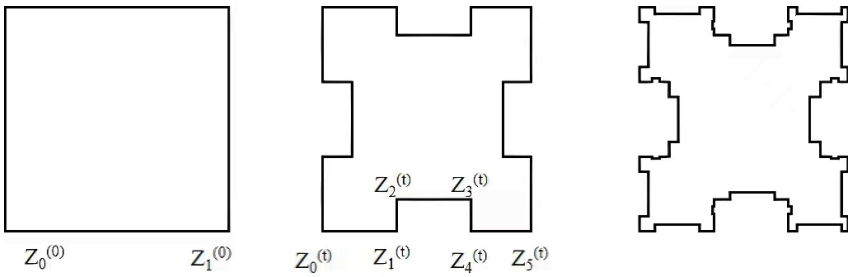

FIGURE 5. Iterations of Minkowski fractal structure.

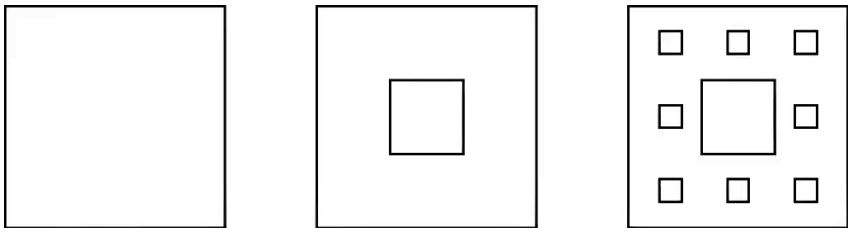

FIGURE 6. Iterations of Sierpinski fractal structure.

magnitude and phase angle:

$$\begin{aligned} Z_5^{(1)} &= re^{j\theta_0} + Z_0^{(1)} \\ Z_1^{(1)} &= \frac{1}{3} re^{j(\theta_0+\theta_1)} + Z_0^{(1)} \\ Z_2^{(1)} &= \frac{\sqrt{1+\alpha^2}}{3} re^{j(\theta_0+\theta_2)} + Z_0^{(1)} \\ Z_3^{(1)} &= \frac{\sqrt{4+\alpha^2}}{3} re^{j(\theta_0+\theta_3)} + Z_0^{(1)} \\ Z_4^{(1)} &= \frac{2}{3} re^{j(\theta_0+\theta_4)} + Z_0^{(1)} \end{aligned} \tag{3}$$

In the equation, $\theta_0 = \theta_4 = 0$ and $\theta_0 = \arctan(\alpha/2)$. The parameter α represents the depth of the notches, and different values of α affect the fractal dimension, which in turn determines the filling capacity of the fractal structure. Therefore, the depth of the notches α and the total perimeter of the fractal loop collectively determine the filling area of the fractal loop. Next, by replacing the initial unit with the generating unit, a first-order Minkowski curve can be obtained. By varying the value of α, different forms of first-order Minkowski curves can be generated. All straight edges of M_1 are replaced with the generating unit, and the iteration continues with the same α value to generate the second-order Minkowski curve M_2. Four Minkowski curves form a Minkowski fractal loop, creating an ideal second-order Minkowski fractal curve that is continuous and non-differentiable at every point.

The core of Sierpinski fractal theory involves dividing the initial rectangular patch into nine equally sized smaller rectangles and removing the central one. During the second iteration, the central small rectangles of the remaining eight are further removed, with each removed small rectangle having an area of $\frac{1}{9}$ of the initial central rectangle's area [21], as shown in Fig. 6. Assuming that the initial rectangular patch has an area of $A_0 = 10$ mm $\times 10$ mm, the area after n iterations of the Sierpinski fractal can be expressed as $A_n = \left(\frac{8}{9}\right)^n \times A_0$. From the expression for the antenna area, it is evident that as the number of iterations n increases, the antenna area gradually decreases approaching zero as n tends to infinity.

Figure 7 illustrates the distribution characteristics of the antenna's surface current. It is observed that the direction of the surface current varies with the feed phase angle. Specifically, when the feed phase angle is 0°, the current vector primarily flows along the $+y$-axis direction; at a 90° feed phase angle, the current vector deflects towards the $-x$-axis direction; under a 180° feed phase angle, the current direction shifts to the $-y$-axis direction; and at a 270° feed phase angle, the current is predominantly concentrated along the $+x$-axis direction. This phase variation results in a counterclockwise rotation of the surface current when being viewed from the $+z$-axis direction, with the radiated electric field vector also rotating counterclockwise in a circular manner. According to the right-hand rule, the antenna is identified as an RHCP antenna.

2.3. Parameter Study

During the antenna design process, to achieve its optimal performance, it is essential to meticulously optimize the relevant parameters. In this design, the particularly critical performance indicators include resonant frequency and axial ratio. Specifically, the key parameters that cause the resonant frequency to shift towards lower frequencies, thereby enabling antenna miniaturization, are primarily α, l_x, l_y, and W_1, whereas the parameter that has the most significant impact on the axial ratio is d.

Figure 8 illustrates that as the frequency increases, the axial ratio of antennas with various notched dimensions follows

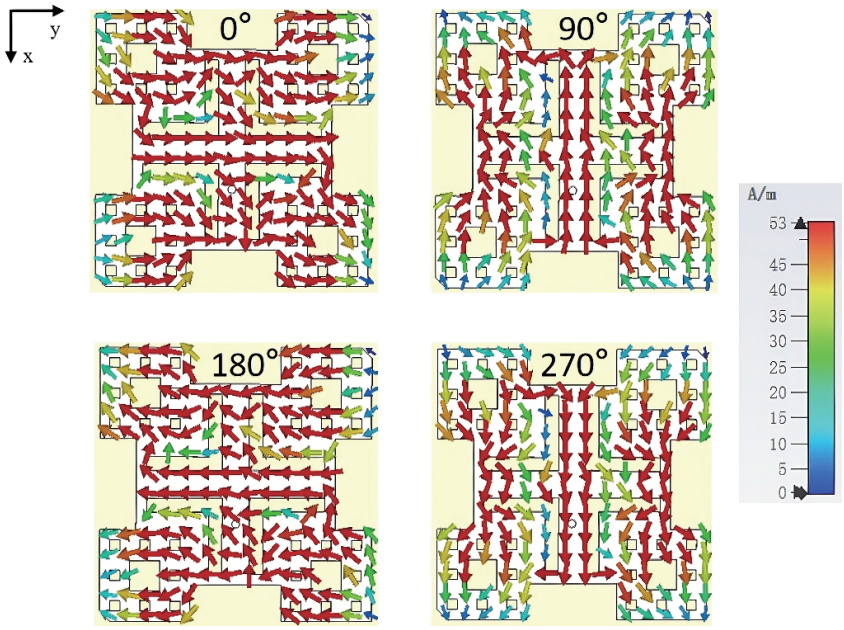

FIGURE 7. Surface current of the proposed antenna with different phases.

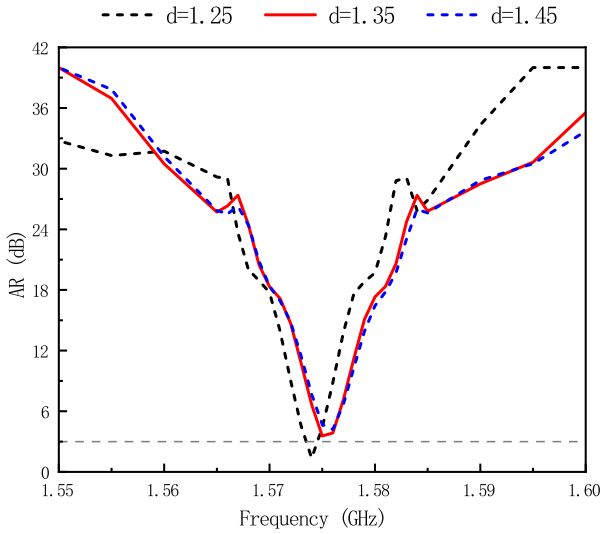

FIGURE 8. Simulated AR of the proposed antenna with different: d.

a pattern of initially decreasing and then increasing. Around 1.575 GHz, all curves reach their minimum points, with the antenna having a notched dimension of $d = 1.25$ exhibiting the lowest axial ratio, approaching 0 dB. This indicates that at this particular notched dimension, the antenna's performance is optimal. As the notched dimension increases, the minimum point of the axial ratio slightly increases, but the overall trend remains consistent. Additionally, the graph shows that near 1.57 GHz, the antenna with $d = 1.25$ has a significantly better axial ratio than the other two dimensions, suggesting that reducing the notched dimension helps to lower the antenna's axial ratio, thereby enhancing its radiation performance.

As depicted in Fig. 9(a), the resonant frequency of the antenna gradually decreases with the increase in parameter α. Concurrently, the axial ratio exhibits a similar trend to the frequency but with more pronounced fluctuations. For instance, when α is set to 0.39, the performance of axial ratio drops to 6 dB, which is approximately 3 dB lower than that when α is 0.4. This suggests that the depth of the Minkowski fractal notch, represented by α, has a notable impact on the antenna's CP performance. Fig. 9(b) and Fig. 9(c) illustrate the effects of the length (l_x) and width (l_y) of the L-shaped slot at the antenna's center on its performance. According to the theory presented in Section 2.2, increasing the length of the slot extends the current path, thereby causing the resonant frequency to shift

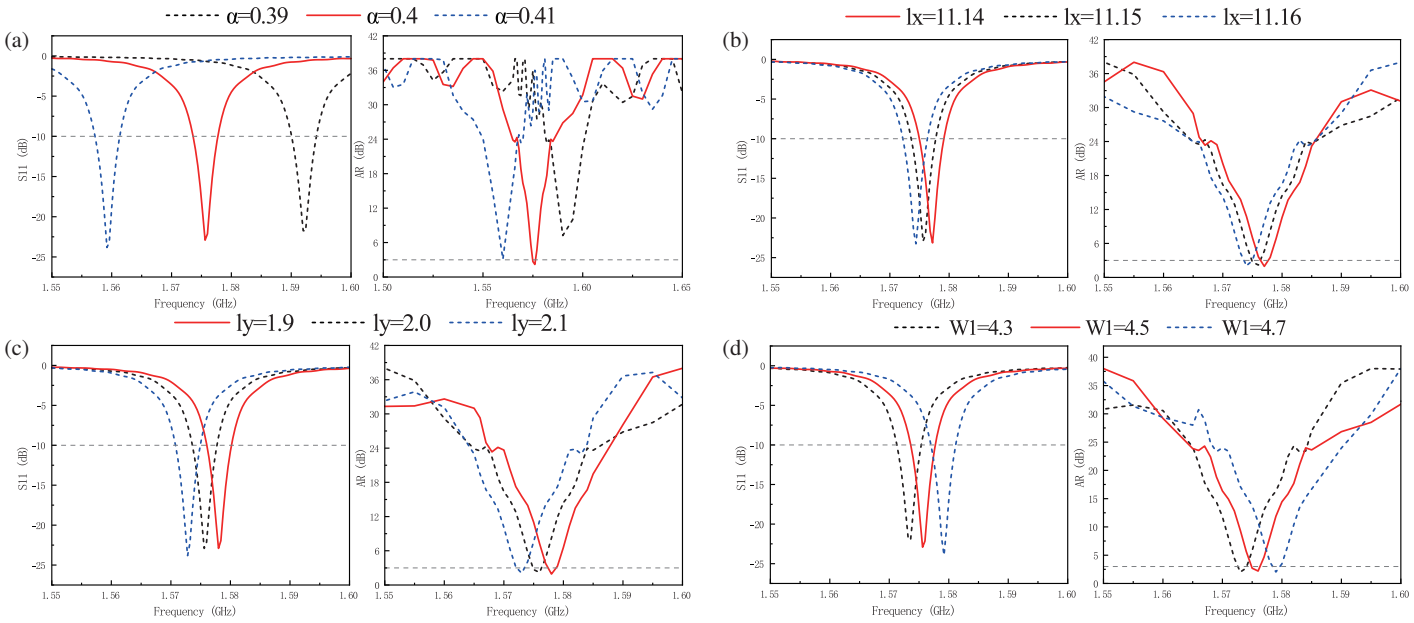

FIGURE 9. Simulated S_{11} and AR of the proposed antenna with different: (a) α. (b) lx. (c) ly. (d) W_1.

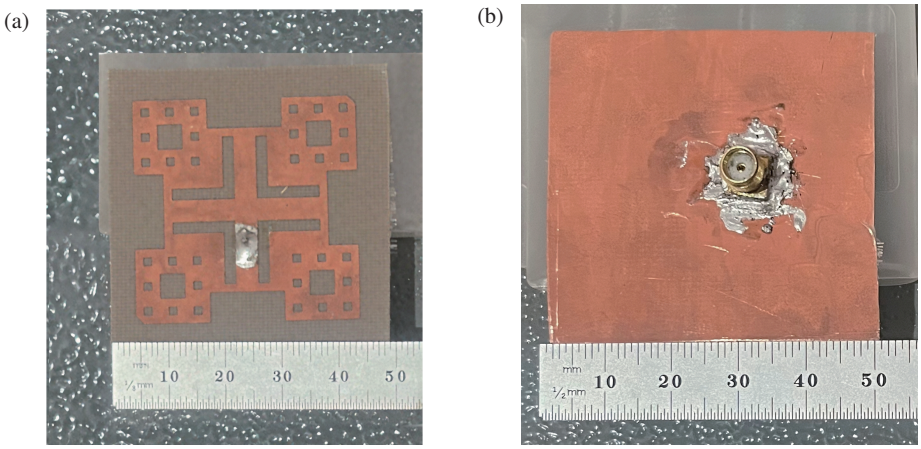

FIGURE 10. Photograph of the fabricated prototype. (a) Top view. (b) Bottom view.

towards lower frequencies, a phenomenon that is corroborated by the simulation results. As l_x and l_y increase, the frequency of the resonance progressively decreases, with changes in l_x having a more significant effect. Additionally, these two parameters have a consistent impact on the axial ratio. However, during the parameter variation process, both the axial ratio bandwidth and axial ratio value remain relatively stable, indicating minimal influence on the CP performance.

As observed in Fig. 9(d), the resonant frequency of the antenna tends to shift towards higher frequencies with the increase of parameter W_1. Concurrently, the reflection coefficient S_{11} decreases with the rising frequency, indicating an improvement in the antenna's impedance matching performance. Additionally, the antenna's axial ratio also shifts towards higher frequencies with the increase of W_1, yet its axial ratio performance remains relatively stable despite the changes in W_1. In summary, the opening size W_1 of the Sierpinski fractal structure significantly affects the antenna's impedance matching performance, while its impact on the CP performance is comparatively minimal.

3. MEASUREMENT RESULTS

To validate the effectiveness of the designed antenna, as shown in Fig. 10, we fabricated a physical prototype of the antenna. The S-parameters of the antenna were precisely measured using AV3629A integrated vector network analyzer. Additionally, in an anechoic chamber environment, detailed measurements of the antenna's 2D gain pattern and axial ratio were conducted. These test results provide crucial data support for evaluating the antenna's performance.

As shown in Fig. 11, the graph presents a comparison between the simulated and measured results of the antenna's S_{11}

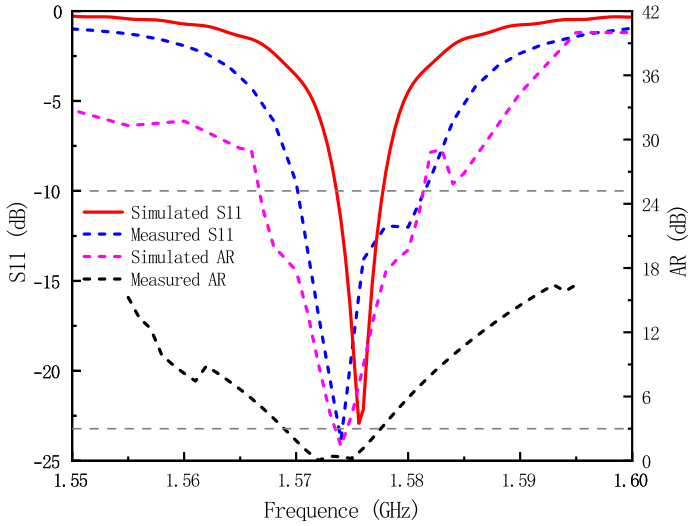

FIGURE 11. Comparisons of S_{11} and AR between measured one and simulated one.

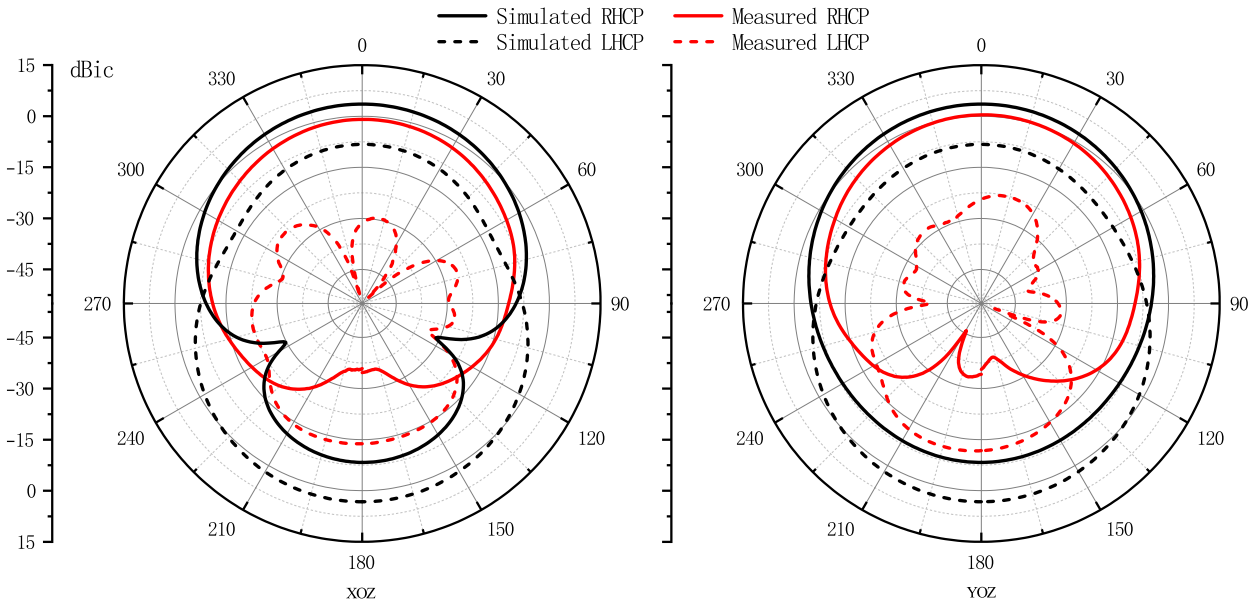

FIGURE 12. Simulated and measured radiation patterns at 1.575 GHz.

and axial ratio. It can be observed that the measured results are optimized compared to the simulated ones. By comparing the red and blue lines, it is evident that the center frequency of the measured antenna has shifted towards lower frequencies relative to the simulated results. However, the bandwidth has expanded from the simulated range of 1.573 GHz to 1.578 GHz (5 MHz) to the measured range of 1.57 GHz to 1.582 GHz (12 MHz). Simulation validation analysis indicates that the primary cause of this discrepancy is manufacturing errors. The designed antenna employs a coaxial feed structure, where the parameters of the inner and outer conductor radii of the coaxial line both influence the antenna's resonant frequency. During the manufacturing process, limitations in conditions led to discrepancies between the fabricated antenna and simulated one, resulting in differences between the test and simulation results.

In Fig. 11, the pink and black lines correspond to the simulated and measured axial ratios, respectively. The measured axial ratio bandwidth is notably wider than the simulated data. The simulated bandwidth spans from 1.573 GHz to 1.576 GHz (3 MHz), whereas the measured bandwidth extends from 1.569 GHz to 1.578 GHz (9 MHz). This suggests that the actual antenna's CP performance surpasses the simulation. The improvement could be attributed to refinements in the antenna's structure during manufacturing and the enhanced material properties in real-world applications, both of which contribute to the improved CP characteristics.

Figure 12 presents a comparison of the simulated and measured two-dimensional radiation patterns for left hand circular

TABLE 2. Comparison of proposed antenna design with literature.

Designed Antenna	Size of Antenna	Center Resonant Frequency	S_{11} bandwidth	AR bandwidth	Substrate
[6]	60 mm × 60 mm × 5 mm	1575 MHz	90 MHz	35 MHz	($\varepsilon_r = 3.40$)
[7]	70 mm × 70 mm × 2 mm	1575 MHz	72 MHz	47 MHz	FR-4 ($\varepsilon_r = 4.52$)
[8]	36 mm × 36 mm × 1.524 mm	2400 MHz	59 MHz	12 MHz	RO4003C ($\varepsilon_r = 3.38$)
[14]	52 mm × 52 mm × 3.2 mm	2225 MHz	120 MHz	90 MHz	Rogers5880 ($\varepsilon_r = 2.20$)
[22]	90 mm × 90 mm × 4.572 mm	910 MHz	18 MHz	6 MHz	RO4003C ($\varepsilon_r = 3.48$)
[23]	90 mm × 90 mm × 4.572 mm	930 MHz	19 MHz	6 MHz	RO4003C ($\varepsilon_r = 3.38$)
Proposed	**50 mm × 50 mm × 0.762 mm**	**1575 MHz**	**12 MHz**	**9 MHz**	**TLX-8 (ε_r= 2.55)**

polarization (LHCP) and RHCP of the antenna in the XOZ and YOZ planes. In the XOZ plane, the measured results show a difference of 28.5 dBi between the maximum directivity of the main polarization and the cross polarization, while in the YOZ plane, this difference is 24.6 dBi, indicating that the axial ratio is below 3 dB in both cases. Notably, at 1.575 GHz, the measured axial ratio is only 0.197 dB, demonstrating excellent CP performance. Additionally, the maximum directivity gain of the measured antenna reaches 0.39 dBi. Overall, the measured radiation patterns closely align with the simulated ones, validating the effectiveness of the antenna design.

Despite the deviations observed between the theoretical computations and empirical measurements, the microstrip antenna design methodology introduced in this study exhibits notable superiority over the techniques reported in the existing literature [6–8, 14, 22, 23]. A detailed comparison of the proposed antenna with alternative design strategies is presented in Table 2. Compared with other antennas in the literature, the proposed antenna achieves a distinct advantage in terms of compactness. Moreover, it has a relatively narrow bandwidth, which endows it with a stronger selectivity for specific frequencies. As a result, it can better suppress signals at non-resonant frequencies, thereby reducing interference and enhancing the quality and reliability of the signals. The simulation outcomes suggest that this antenna can be effectively integrated into more compact systems, thereby expanding its potential applications in scenarios such as aircraft navigation.

4. CONCLUSION

This study presents the design and development of a compact CP antenna incorporating four L-shaped slots and an M-S fractal geometry. Utilizing this innovative structural configuration, the size of the antenna has been reduced by 54.3% compared to conventional antennas. A detailed comparison between simulated and experimental data is conducted to thoroughly investigate its impedance characteristics and radiation mechanisms. The antenna operates within a frequency range of 1.57 GHz to 1.582 GHz, demonstrating exceptional anti-interference performance in this band. Within the 1.569 GHz to 1.578 GHz frequency interval, the axial ratio remains below 3 dB, ensuring high polarization purity, while the maximum directional gain reaches 0.39 dBi. The strong agreement between measured and simulated results validates the reliability of the design. In addition to miniaturization, the antenna offers advantages such as a simplified structure, low cost, and a low-profile form factor. It maintains stable radiation characteristics and is ideally suited for GPS applications, effectively advancing modern technology toward higher levels of integration. This work provides practical and viable technical support for the advancement of related fields.

ACKNOWLEDGEMENT

This work was supported by the Natural Science Research Project of Anhui Educational Committee (Grant No: 2024AH051584).

REFERENCES

[1] Kumar, G., P. Mevada, R. C. Gupta, V. K. Singh, S. Kulshrestha, and M. B. Mahajan, "A miniaturized tri-band CP antenna," *Progress In Electromagnetics Research C*, Vol. 150, 187–193, 2024.

[2] Zade, P. L. and S. S. Khade, "Miniaturized novel multi resonance monopole planar antenna with slots, slits, split ring resonator," *Progress In Electromagnetics Research C*, Vol. 145, 75–82, 2024.

[3] Sundarsingh, E. F., A. Harshavardhini, *et al.*, "A compact conformal windshield antenna for location tracking on vehicular platforms," *IEEE Transactions on Vehicular Technology*, Vol. 68, No. 4, 4047–4050, 2019.

[4] Hasan, M. M., M. T. Islam, T. Alam, P. Kirawanich, S. Alamri, and A. S. Alshammari, "Metamaterial loaded miniaturized extendable MIMO antenna with enhanced bandwidth, gain and isolation for 5G sub-6 GHz wireless communication systems," *Ain Shams Engineering Journal*, Vol. 15, No. 12, 103058, 2024.

[5] Chen, Z. N., X. Qing, *et al.*, "Asymmetric-circular shaped slotted microstrip antennas for circular polarization and RFID applications," *IEEE Transactions on Antennas and Propagation*, Vol. 58, No. 12, 3821–3828, 2010.

[6] Qing, X., Z. N. Chen, *et al.*, "A compact circularly polarized slotted patch antenna for GNSS applications," *IEEE Transactions on Antennas and Propagation*, Vol. 62, No. 12, 6506–6509, 2014.

[7] Ma, Z. and X. Huang, "Design of a circularly polarized microstrip antenna for aircraft tracking based on beidou III compatible with multi-navigation system," *Micromachines*, Vol. 14, No. 11, 2083, 2023.

[8] Qing, X., Z. N. Chen, *et al.*, "Compact asymmetric-slit microstrip antennas for circular polarization," *IEEE Transactions on Antennas and Propagation*, Vol. 59, No. 1, 285–288, 2010.

[9] Nasimuddin, X. Qing, and Z. N. Chen, "Compact circularly polarized symmetric-slit microstrip antennas," *IEEE Antennas and Propagation Magazine*, Vol. 53, No. 4, 63–75, 2011.

[10] Karimbu Vallappil, A., M. K. A. Rahim, B. A. Khawaja, M. N. Iqbal, N. A. Murad, M. M. Gajibo, L. O. Nur, and B. S. Nugroho, "Complementary split-ring resonator and strip-gap based metamaterial fractal antenna with miniature size and enhanced bandwidth for 5G applications," *Journal of Electromagnetic Waves and Applications*, Vol. 36, No. 6, 787–803, 2022.

[11] Abed, A. T. and A. M. Jawad, "Compact size MIMO amer fractal slot antenna for 3G, LTE (4G), WLAN, WiMAX, ISM and 5G communications," *IEEE Access*, Vol. 7, 125 542–125 551, 2019.

[12] Mandelbrot, B. B., *The Fractal Geometry of Nature*, Vol. 8, 406–406, H. B. Fenn and Company Ltd., 1983.

[13] Paun, M.-A., M.-V. Nichita, V.-A. Paun, and V.-P. Paun, "Minkowski's loop fractal antenna dedicated to sixth generation (6G) communication," *Fractal and Fractional*, Vol. 6, No. 7, 402, 2022.

[14] Raj, A., D. C. Dhubkarya, D. K. Srivastava, and D. Mandal, "Design and analysis of square shape slot cut high gain Sierpinski carpet fractal antenna for wireless applications," *Microwave and Optical Technology Letters*, Vol. 65, No. 8, 2337–2343, 2023.

[15] Pandav, S., G. Sadhukhan, T. K. Das, S. K. Behera, and M. Mohanty, "Circularly polarized high gain Koch fractal antenna for space applications," *Sādhanā*, Vol. 47, No. 4, 276, 2022.

[16] Jaffri, Z. U. A., Z. Ahmad, A. Kabir, and S. S. H. Bukhari, "A novel miniaturized Koch-Minkowski hybrid fractal antenna," *Microelectronics International*, Vol. 39, No. 1, 22–37, 2022.

[17] Vallappil, A. K., B. A. Khawaja, M. K. A. Rahim, M. Uzair, M. Jamil, and Q. Awais, "Minkowski–sierpinski fractal structure-inspired 2 × 2 antenna array for use in next-generation wireless systems," *Fractal and Fractional*, Vol. 7, No. 2, 158, 2023.

[18] Yuan, J., J. Zheng, and Z. D. Chen, "A compact meandered ring antenna loaded with parasitic patches and a slotted ground for global navigation satellite systems," *IEEE Transactions on Antennas and Propagation*, Vol. 66, No. 12, 6835–6843, 2018.

[19] Prabhakar, H. V., U. K. Kummuri, R. M. Yadahalli, and V. Munnappa, "Effect of various meandering slots in rectangular microstrip antenna ground plane for compact broadband operation," *Electronics Letters*, Vol. 43, No. 16, 848–850, 2007.

[20] Dhar, S., R. Ghatak, B. Gupta, and D. R. Poddar, "A wideband minkowski fractal dielectric resonator antenna," *IEEE Transactions on Antennas and Propagation*, Vol. 61, No. 6, 2895–2903, 2013.

[21] Froumsia, D., E. D. Jean-François, A. Houwe, *et al.*, "Miniaturization of dual bands fractal-based microstrip patch fractal antenna for X and Ku bands applications," *The European Physical Journal Plus*, Vol. 137, No. 6, 746, 2022.

[22] Nasimuddin, Z. N. Chen, and X. Qing, "A compact circularly polarized cross-shaped slotted microstrip antenna," *IEEE Transactions on Antennas and Propagation*, Vol. 60, No. 3, 1584–1588, 2012.

[23] Nasimuddin, Z. N. Chen, and X. Qing, "Compact circularly polarized asymmetric-slotted microstrip patch antennas," *Microwave and Optical Technology Letters*, Vol. 54, No. 8, 1920–1927, 2012.